Chinese Journal of
POLYMER SCIENCE

RESEARCH ARTICLE

https://doi.org/10.1007/s10118-026-3727-1
Chinese J. Polym. Sci.

High-strength and Electrically Stable Aramid Nanofibers/Multi-walled Carbon Nanotubes/Polyaniline Hybrid Fibers for Flexible Electromagnetic Absorption Performance

Xiao-Qi Ni, Xiang-Yang Xu, Yao-Feng Zhu*, and Hui-Ya Wang*

School of Materials Science and Engineering, Zhejiang Sci-Tech University, Hangzhou 310018, China

Electronic Supplementary Information

Abstract The rapid advancement of communication technologies and wearable applications has increased the demand for high-performance flexible electromagnetic wave absorption materials. Conventional conductive fibers are often constrained by their poor wearability, weak interfacial stability, and limited absorption efficiency, which restrict their reliability and practical applicability in dynamic environments. Herein, a flexible and robust electromagnetic-absorbing fiber was successfully fabricated *via* wet spinning techniques, which integrates multi-walled carbon nanotubes (MWCNTs), polyaniline (PANI), and aramid nanofibers (ANFs). Polymerization of PANI on the MWCNTs surface is employed to optimize impedance matching and enhance interfacial compatibility, while ANFs serve as a continuous structural skeleton, improving the mechanical strength and spinnability. The resulting composite fibers exhibited a tensile strength of (202.0±8.0) MPa and an elongation at break of 13.6%±0.9%, stable electrical conductivity under mechanical deformation, and ultrasonic cleaning. Notably, the fiber architecture enables superior electromagnetic wave absorption, achieving a minimum reflection loss of −62.07 dB and an effective bandwidth of 3.24 GHz compared to the powder counterparts, owing to the extended propagation path and multiple scattering within the aligned fiber network. In addition, the composite fibers demonstrated self-extinguishing behavior during combustion, reflecting their inherent flame-retardant characteristics. This study provides a feasible strategy for developing flexible, high-performance electromagnetic wave (EMW)-absorbing fibers for next-generation protective textile materials.

Keywords Microwave absorption performance; Flexible composite fiber; Aramid nanofibers; Polyaniline/multi-walled carbon nanotubes; Electrically stable

Citation: Ni, X. Q.; Xu, X. Y.; Zhu, Y. F.; Wang, H. Y. High-strength and electrically stable aramid nanofibers/multi-walled carbon nanotubes/polyaniline hybrid fibers for flexible electromagnetic absorption performance. *Chinese J. Polym. Sci.* https://doi.org/10.1007/s10118-026-3727-1

INTRODUCTION

The proliferation of modern communication technologies has rendered electromagnetic wave (EMW) radiation an increasingly critical issue,[1,2] as it not only disrupts the normal operation of electronic devices, but also poses a potential threat to human health.[3,4] Long-term exposure to electromagnetic radiation is associated with adverse effects on the nervous, reproductive, and cardiovascular systems, spurring significant interest in high-efficiency EMW absorption materials.[5–7] Compared with conventional rigid absorbers, fabric-based EMW-absorbing materials offer notable advantages, including light weight, high flexibility, wearability, and customizable geometry. These features allow them to closely conform to surfaces that require protection and dynamic operating conditions. thereby broadening their applications in flexible electromagnetic protection.[8–11]

Currently, metal-based conductive fibers are limited by their high rigidity, poor tactile comfort, and susceptibility to oxidation, which compromise the wearing comfort. In addition, their excessively high electrical conductivity hinders efficient electromagnetic wave absorption. In contrast, conductive polymers (*e.g.*, polyaniline, polypyrrole, and polythiophene) possess tunable conductivity, low density, environmental stability, and molecular design flexibility,[12–14] making them promising candidates for EM functional fibers. However, most current preparation methods depend on surface coating[15–17] or chemical deposition[18,19] which often leads to weak interfacial bonding and poor mechanical durability. Under bending or deformation, the conductive layers are susceptible to delamination, resulting in a significant deterioration of the electrical and EMW absorption performance.[20–22] Therefore, realizing a synergistic and stable integration of EM-functional components within the fiber matrix is fundamental for addressing these interfacial limitations.

Wet spinning is a viable strategy for constructing integrat-

* Corresponding authors, E-mail: yfzhu@zstu.edu.cn (Y.F.Z.)
E-mail: hywang@zstu.edu.cn (H.Y.W.)
Received February 28, 2026; Accepted April 25, 2026; Published online August 19, 2026

ed fibers with strong interfacial bonding. An ideal fiber system should achieve a balance between electromagnetic performance and mechanical integrity, which is typically realized through the synergistic incorporation of multiple functional components. In this context, multiwalled carbon nanotubes (MWCNTs) are widely regarded as effective EMW-absorbing fillers owing to their excellent dielectric loss characteristics.[23,24] Meanwhile, introducing a reinforcing phase with favorable mechanical attributes is a key strategy to enhance fiber processability and mechanical strength. Aramid nanofibers (ANFs) retain the high strength, high modulus, and outstanding thermal stability of macroscopic aramid fibers,[25–27] while their nanoscale one-dimensional structure and abundant surface functional groups facilitate superior dispersion in the spinning solution.[28] Through physical entanglement and hydrogen bonding, ANFs improve interfacial adhesion with the matrix material, thereby offering structural reinforcement for the fabrication of continuous, tough, and strongly bonded composite fibers.[29]

In this study, we developed an integrated strategy for fabricating flexible, high-performance EMW-absorbing fibers through wet spinning by selecting ANFs as a structural framework. The multiwalled carbon nanotubes/polyaniline (MWCNT/PANI) composite fillers were prepared by *in situ* polymerization of PANI on MWCNTs, which enabled uniform PANI coating to optimize impedance matching while enhancing interfacial compatibility through covalent and π-π interactions. This multicomponent synergistic design allows the concurrent optimization of both the electromagnetic and mechanical properties within a continuous fiber architecture. The mass ratios of MWCNT-to-PANI and MWCNT/PANI to the ANFs were systematically tailored to balance the fiber morphology, mechanical strength, and EMW absorption performance. This study provides a feasible fabrication pathway for structurally integrated and interface-enhanced functional fibers, along with in-depth mechanistic insights into the absorption behavior of multicomponent fibrous systems.[30]

EXPERIMENTAL

Materials

Aniline (ANi, AR, ≥99.5%), dodecylbenzenesulfonic acid (DBSA, 90%), dimethyl sulfoxide (DMSO, AR), polyvinylpyrrolidone (PVP, MW: 1.3×10^6), potassium hydroxide (KOH, 95%), and methanol (MeOH, AR) were purchased from Aladdin Chemistry Co., Ltd. Multi-walled carbon nanotubes MWCNTs (ID: 3–5 nm, OD: 8–15 nm) were supplied by Shenghui Industrial Co., Ltd. Aramid fibers (Kevlar 49) were obtained from DuPont (USA). Ammonium persulfate (APS, AR, 98.5%) was purchased from Macklin. PDMS (DC 184) was provided by Dow Corning. Ethanol (EtOH, 95 wt%) was purchased from Hangzhou Gaojing Fine Chemical Co., Ltd.

Preparation of MWCNT/PANI

The MWCNT/PANI composite powders were synthesized *via in situ* polymerization. A mixture of PVP and MWCNTs in a mass ratio of 4:1 was dispersed in 150 mL of deionized water *via* ultrasonic treatment for 15 min to obtain a stable dispersion. Separately, 2.51 g of APS) was dissolved in 15 mL of deionized water under magnetic stirring for 10 min. Next, 3.59 g of DBSA) was added to the MWCNT dispersion and stirred for 15 min, followed by dropwise addition of 1.00 g of aniline monomer. After further stirring for 15 min to ensure homogeneity, APS solution was added dropwise to initiate polymerization. The reaction was maintained under continuous stirring for 10 h. Upon completion, ethanol was added to break the emulsion, and the mixture was centrifuged and washed for thrice with ethanol and deionized water. The final product was freeze-dried for 7 days to yield MWCNT/PANI composite powders. Samples prepared with different MWCNT-to-aniline mass ratios (1:1, 1:2, 1:4, and 1:8) are denoted as CP11, CP12, CP14, and CP18, respectively.

Preparation of ANF/MWCNT/PANI Composite Fibers

First, 2.4 g of aramid fiber was cut into 3 cm segments and treated in methanol by ultrasonication for 30 min. The fibers were then thoroughly washed with deionized water and dried. The cleaned aramid fibers were mixed with KOH (3.6 g), DMSO (150 mL), and deionized water (4 mL) and stirred at room temperature for 5 h, yielding a viscous dark-red dispersion of aramid nanofibers (ANFs). Subsequently, a certain amount of MWCNT/PANI composite powder was added to the ANF dispersion and stirred at room temperature for 18 h, followed by ultrasonic defoaming for 30 min to obtain a homogeneous spinning doping.

The spinning solution was extruded through a flat-tip needle (inner diameter 0.41 mm, 22 G) using a syringe pump at a rate of 10 mL/h in a deionized water coagulation bath. The nascent fibers were thoroughly washed with deionized water to remove any residual impurities. The fibers were then collected using a winding device and thermally treated in a vacuum oven at 50 °C to obtain the ANF/MWCNT/PANI composite fibers. Based on the mass ratio of MWCNT/PANI to ANF (1:1, 2:1, and 3:1), the resulting fibers were labeled as 1ACP, 2ACP, and 3ACP, respectively.

Characterization

Field-emission scanning electron microscopy (FESEM, Ultra 55) was used to analyze the surface structures of the samples. Fourier transform infrared spectroscopy (FTIR, Thermo Electron Corp.) and X-ray diffraction (XRD, Bruker, D8 Discover, 10°–80°) were employed to analyze the functional groups and crystalline structure, respectively. The mechanical properties were measured using an electronic single-fiber strength meter (YG004) at a strain rate of 20 mm/min over a gauge length of 20 mm. Thermal stability was evaluated by thermogravimetric analysis (TG, Netzsch TG 209 F3 Tarsus) under a nitrogen atmosphere from room temperature to 800 °C at 10 °C/min. A vector network analyzer (N5222A, Keysight) was used to measure the electromagnetic parameters. The MWCNT/PANI composite sample was uniformly mixed with paraffin wax at a filler content of 5 wt% and pressed into a coaxial ring with an inner diameter of 3.04 mm and an outer diameter of 7.00 mm. In the waveguide measurement, the ANF/MWCNT/PANI composite fibers were closely aligned and encapsulated with PDMS, with their fiber axes oriented parallel to the direction of the electric field (E-field) within the rectangular waveguide.

RESULTS AND DISCUSSION

Morphology and Structure of ANF/MWCNT/PANI Composite Fiber

Fig. 1(a) illustrates the fabrication process of ANF/MWCNT/PANI composite fibers. Initially, the MWCNT/PANI composites are syn-

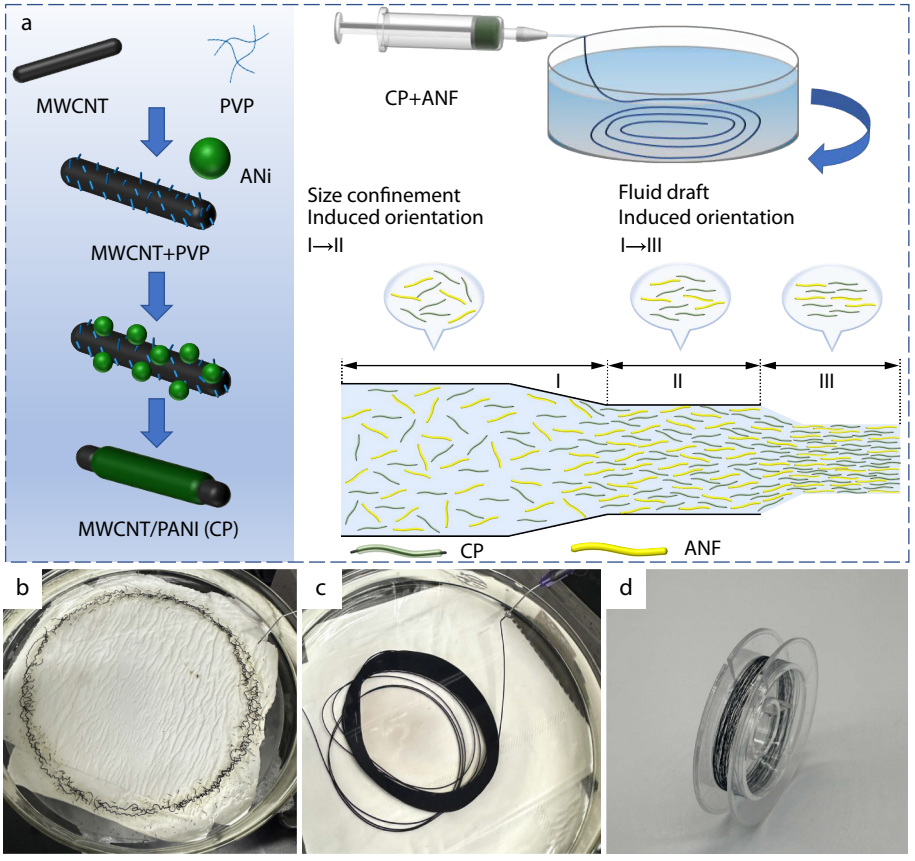

Fig. 1 Wet-spinning process of (a) MWCNT/PANI and (b) ANF/MWCNT/PANI composites; (c) Photograph of ANF/MWCNT/PANI composite fiber; (d) Preparation process diagram of ANF/MWCNT/PANI composite fiber.

thesized *via in situ* polymerization and subsequently mixed with ANF to form a spinning solution. During the wet-spinning process, the gradually narrowed spinning channel generates strong shear forces to align and orient the MWCNT/PANI and ANF components along the flow direction.[31] The extruded fibers are then solidified in a coagulation bath and collected. As shown in Fig. 1(b), the MWCNT/PANI composite suffers from poor processability, insufficient mechanical strength, and discontinuous fiber formation during the wet spinning process, largely owing to weak interparticle cohesion and the absence of a continuous structural framework. ANFs were introduced as a reinforcing and fiber-forming matrix to create a spinnable ANF/MWCNT/PANI hybrid system, overcoming these limitations. In this design, ANFs serve not only as a mechanical scaffold that enhances cohesion and stretchability during spinning but also as a nanoscale binder that improves the dispersion and interfacial stress transfer between the conductive fillers. As shown in Figs. 1(c) and 1(d), the resulting composite enables continuous and uniform fiber extrusion with stable morphology and structural integrity throughout the wet spinning process. These results indicate that the system possesses good spinnability and practical application potential, providing a feasible foundation for large-scale fabrication of flexible conductive fiber materials.

FTIR spectroscopy was performed to identify functional groups, as illustrated in Fig. 2(a). The absorption bands at 1564 and 1487 cm^{-1} are attributed to the stretching vibrations of the C=C bonds in the quinoid and benzenoid rings, respectively. The bands at 1300 and 1247 cm^{-1} correspond to the C—N stretching vibrations in aromatic amines and C—N^+ bonds in the doped polyaniline backbone, respectively, indicating that the synthesized PANI chains exhibit a conductive state. In addition, the bands observed at 1130 and 794 cm^{-1} are assigned to the in-plane and out-of-plane bending vibrations of C—H bonds, confirming the successful synthesis of polyaniline.[32] As shown in Fig. 2(b), the XRD pattern of the MWCNT/PANI composite exhibits a distinct peak at 25.1°, which corresponds to the (002) diffraction plane of graphitic carbon in the MWCNTs. Another peak observed near 42.8° is attributed to the (100) plane of graphite, indicating that the graphitic crystalline structure of the MWCNTs was well preserved during the preparation process. Additionally, the characteristic peaks at approximately 15.2° and 20.2° are assigned to the (011) and (020) planes of PANI in its emeraldine salt form, respectively.[33] These results confirm the successful combination of the MWCNTs and PANI. The morphological evolution of the MWCNTs and composite was investigated using SEM, as shown in Figs. 3(a)–3(f). As depicted in Figs. 3(a) and 3(b), the pristine MWCNTs display a uniform nanofibrous network with smooth surfaces and diameters of approximately 50–80 nm. With increasing PANI content, the composite fibers exhibit a gradual increase in diameter, indicating the deposition of thicker PANI coatings on the MWCNTs. Meanwhile, the interstitial spaces between the nanotubes became progressively filled with PANI deposits, whereas the one-

https://doi.org/10.1007/s10118-026-3727-1

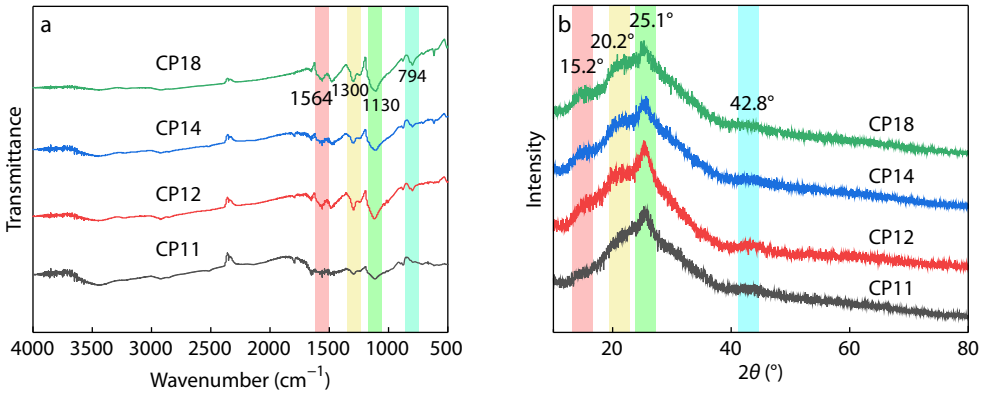

Fig. 2 (a) FTIR spectra, and (b) XRD patterns of MWCNT/PANI composites.

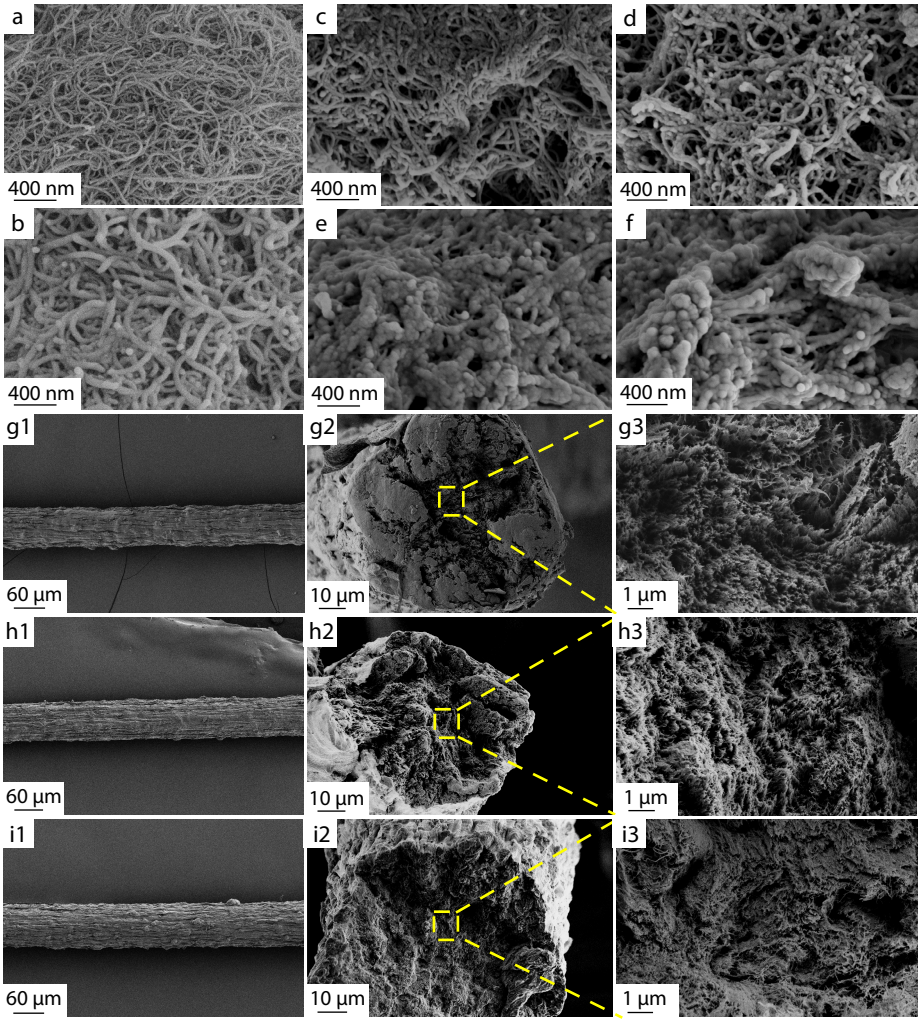

Fig. 3 SEM images of (a, b) MWCNTs, (c) CP11, (d) CP12, (e) CP14, (f) CP18, (g1–g3) 1ACP, (h1–h3) 2ACP, and (i1–i3) 3ACP.

dimensional fibrous morphology of the MWCNTs remains largely intact. Notably, the surfaces of the MWCNTs become rough and uneven, with visible agglomeration of PANI nanoparticles, leading to a marked increase in the surface roughness (Figs. 3a–3f). For the ACP composite fibers in Figs. 3(g1)–(i3), all fibers exhibit a nearly circular cross-section with a dense interior. Both the MWCNT/PANI functional fillers and the ANF matrix are oriented along the fiber axis, forming a highly ordered alignment that promotes close interfiber contact and enhances the macroscopic mechanical properties. With increasing MWCNT/PANI content, the fiber diameter shows a slight enlargement, generally ranging between 70–80 μm with relatively uniform thickness. Additionally, pronounced surface wrinkles can be observed on the fibers,

which could be attributed to rapid water evaporation during the drying process. This sudden shrinkage likely generates compressive stress in the fiber shell, leading to the formation of a wrinkled surface morphology.

Mechanical Property of ANF/MWCNT/PANI Composite Fiber

Fig. 4(a) compares the stress-strain curves of the pure ANF and ACP composite fibers. Neat ANF fibers exhibit excellent mechanical properties, with a tensile strength of up to (431.0±12.0) MPa and a fracture strain of 19.9%±1.4%. As the MWCNT/PANI filler content increased, both the tensile strength and elongation at break of the composite fibers gradually decrease, on account of the reduced continuous high-strength ANF skeleton. Nevertheless, the 3ACP composite fibers still demonstrate favorable overall mechanical performance, with a tensile strength of (138.0±3.0) MPa and a fracture strain of 11.6%±0.7%. Intuitively, a single 3ACP fiber can stably suspend a 100 g weight without breakage, indicating that the fiber maintains good structural integrity and load-bearing capacity (Fig. 4b).

Figs. 4(c) and 4(d) illustrate the variations in the electrical resistance and conductivity of the composite fibers with different MWCNT/PANI contents. The electrical conductivity of the fibers increases with MWCNT/PANI content, following the percolation behavior. In the case of 1ACP fibers, although conductive fillers are introduced, a continuous conductive network has not yet formed within the fiber matrix, resulting in a relatively high resistance and limited improvement in electrical conductivity. With further increases in the MWCNT/PANI content, the conductive filler concentration in the 2ACP and 3ACP fibers exceeds the percolation threshold, leading to the formation of conductive pathways. As a result, the electrical resistance decreases markedly, and the conductivities reach 3.67 and 4.97 S/m, respectively. These results indicate that the MWCNT/PANI functional components establish relatively continuous electron transport networks within the fibers, enabling efficient charge transfer. In electromagnetic wave-absorbing materials, the stability of electrical properties is essential for maintaining effective EMW absorption performance. Disruption of the conductive network, such as broken pathways, coating detachment, or interfacial separation, can reduce conductivity and weaken dielectric loss. To evaluate the electrical stability of the ACP fibers, repeated bending tests over 200 cycles and ultrasonic washing for 50 min were performed. As shown in Figs. 4(e) and 4(f), the ACP composite fibers exhibit relatively consistent conductivity, even after these treatments. Throughout the entire testing process, the conductivity of the 3ACP fiber remains between 4.8 and 5.1 S/m, while that of the 2ACP fiber stays within the range of 3.7–3.9 S/m, indicating excellent retention of electrical performance.

Thermal Property of ANF/MWCNT/PANI Composite Fiber

Fig. 5(a) shows the thermogravimetric curve of the ACP composite fibers. The initial weight loss of the fiber is attributed to the evaporation of residual moisture or solvent from the fiber. The fiber undergoes a significant weight loss in the range of 390–560 °C, mainly because of the thermal decomposition process of the PANI and ANF main chains in the composite system. In this temperature range, PANI undergoes deammoniation, chain scission, and carbonization transformation reactions, resulting in weight loss. The residual mass of the ACP composite fibers is 49.1% at 800 °C. The combustion behaviors and structural changes of conventional cotton threads and ACP composite fibers under high-temperature flame conditions are compared using an alcohol lamp combustion test. As shown in Fig. 5(b), the conventional cotton thread ignites rapidly upon contact with the flame and burns completely within approximately 2 s. In contrast, the ACP composite fibers display good self-ex-

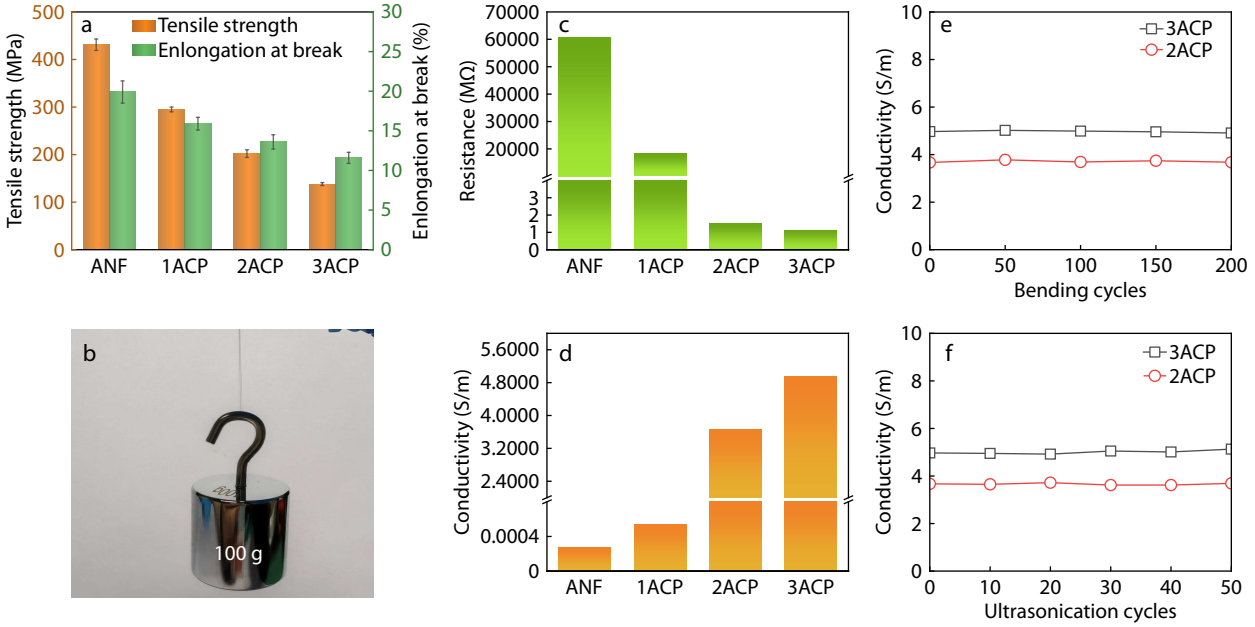

Fig. 4 (a) Breaking strength and elongation of anf/mwcnt/pani composite fiber, (b) photograph of the fiber suspending a weight, (c) electrical resistance, (d) electrical conductivity of fiber, electrical conductivity variation after (e) bending deformation and (f) ultrasonic washing.

https://doi.org/10.1007/s10118-026-3727-1

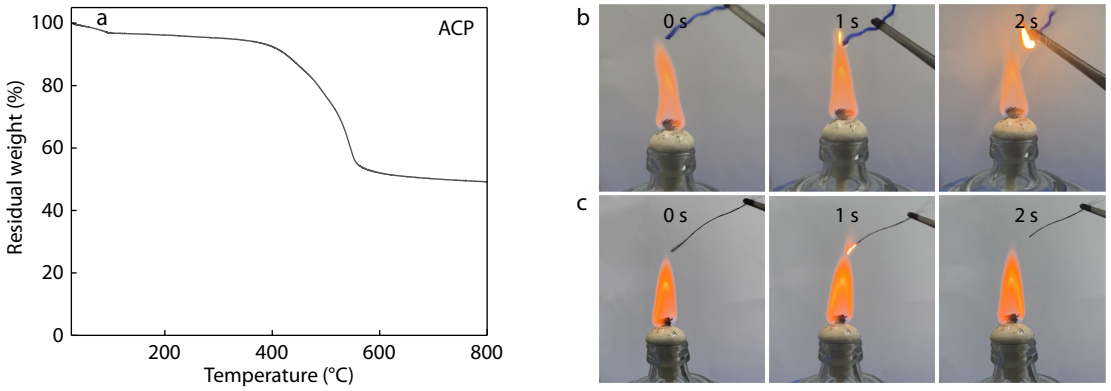

Fig. 5 (a) Thermogravimetric curve of fiber; Combustion test: (b) cotton thread, (c) ACP composite fiber

tinguishing characteristics under identical conditions. In Fig. 5(c), minimal charring is observed after 1 s of flame exposure, with no evidence of vigorous combustion. Upon removal of the flame source, the ACP fibers extinguish immediately, showing no sustained burning. These results demonstrate that the ACP composite fibers possess inherent flame-retardant and self-extinguishing properties, which are mainly ascribed to the excellent thermal stability and intrinsic flame resistance of the ANFs.[34] In addition, MWCNTs and PANI undergo carbonization at elevated temperatures, generating a stable carbonized layer that effectively suppresses flame propagation.

Microwave Absorption Performance of ANF/MWCNT/PANI Composite Fiber

The microwave absorption performance of materials can be evaluated intuitively by reflection loss (RL), which can be represented using the following equation based on transmission line theory:

$$RL = 20\lg\left|\frac{Z_{in}-Z_0}{Z_{in}+Z_0}\right| \quad (1)$$

$$Z_{in} = Z_0\sqrt{\frac{\mu_r}{\varepsilon_r}}\tanh\left(j\frac{2\pi fd\sqrt{\mu_r\varepsilon_r}}{c}\right) \quad (2)$$

where Z_{in} and Z_0 are the input and free-space impedances (Ω), respectively. μ_r and ε_r are the complex permeability and permittivity, respectively. f, d, and c represent the frequency (Hz), thickness (m), and speed of light (m/s), respectively. For dielectric lossy absorbing materials, μ' and μ'' are approximately 1 and 0, respectively.[35] The electromagnetic wave (EMW) absorption characteristics of functional fillers were initially examined to clarify the intrinsic limitations and synergy potential within the integrated system, thereby facilitating the rational design of composite fibers. According to Fig. S1 (in the electronic supplementary information, ESI), neither pure MWCNT nor PANI demonstrates effective electromagnetic wave absorption across the tested frequency range. This is attributed to the high electrical conductivity of the MWCNT, which easily induces a strong skin effect, along with the relatively low attenuation constant of PANI. Ideally, the EMW absorption performance can be enhanced by combining MWCNT with PANI, where the minimum reflection loss (RL_{min}) first decreases and then increases with increasing PANI content (Figs. 6a–6d). Specifically, CP12 exhibits the lowest RL_{min} value (−47.25 dB at a thickness of 2.7 mm, along with an effective absorption bandwidth (EAB) of 5.20 GHz. This is primarily because the electromagnetic wave absorption involves two sequential processes. The first is the efficient introduction of the incident wave into the material, which requires minimizing the reflection at the material-air interface. The second is the sufficient dissipation and attenuation of electromagnetic energy within the bulk material. Therefore, high-performance electromagnetic wave absorbers must exhibit excellent impedance matching and strong attenuation capability, which can be expressed by the following equations:

$$Z = \left|\frac{Z_{in}}{Z_0}\right| = \sqrt{\frac{\mu_r}{\varepsilon_r}}\tanh\left(\frac{j2\pi fd}{c}\sqrt{\mu_r\varepsilon_r}\right) \quad (3)$$

$$\alpha = \frac{\sqrt{2}\pi f}{c}\sqrt{(\mu''\varepsilon'' - \mu'\varepsilon') + \sqrt{(\mu''\varepsilon'' - \mu'\varepsilon')^2 + (\mu'\varepsilon'' + \mu''\varepsilon')^2}} \quad (4)$$

A Z value close to 1 indicates better impedance matching, which is a fundamental prerequisite for achieving efficient electromagnetic wave absorption.[36,37] As shown in Fig. S2(a) (in ESI), the Z values of CP12 calculated at 2.7 mm are closer to 1 across the tested frequency range, suggesting superior impedance matching performance. In contrast, although CP14 and CP18 exhibit higher α values due to the increased PANI content, their Z values deviate significantly from 1, resulting in strong surface reflection and limited wave penetration. The α values of the MWCNT/PANI composites gradually decrease with increasing PANI content (Fig. S2b in ESI), indicating a weakening of the attenuation capability of the electromagnetic waves. Therefore, CP12 achieves the optimal balance between impedance matching and attenuation capability and the best absorption performance among all samples, which is selected as the filler for fiber fabrication.

Figs. 6(e)–6(g) present the reflection loss (RL) curves of the composite fibers with varying MWCNT/PANI contents in the X-band (8.2–12.4 GHz) and Ku-band (12.4–18.0 GHz). The RL_{min} peak gradually shifts toward lower frequencies as the MWCNT/PANI loading increases. Specifically, the 1ACP and 3ACP fibers exhibit a RL_{min} of −31.41 and −65.70 dB at 17.78 and 8.40 GHz with a thickness of 4.85 and 2.28 mm, corresponding to an EAB of 1.68 and 2.11 GHz, respectively. Notably, the 2ACP fiber demonstrates the best performance achieving an RL_{min} of −62.07 dB at 9.20 GHz and an EAB of 3.24 GHz with a thickness of 2.34 mm. The electromagnetic wave absorption performance of the composite fibers aligns with their electrical conductivity behavior (Fig. 4d). Increasing the MWCNT/PANI content promotes the formation of a conductive network within the fibers, which enhances the

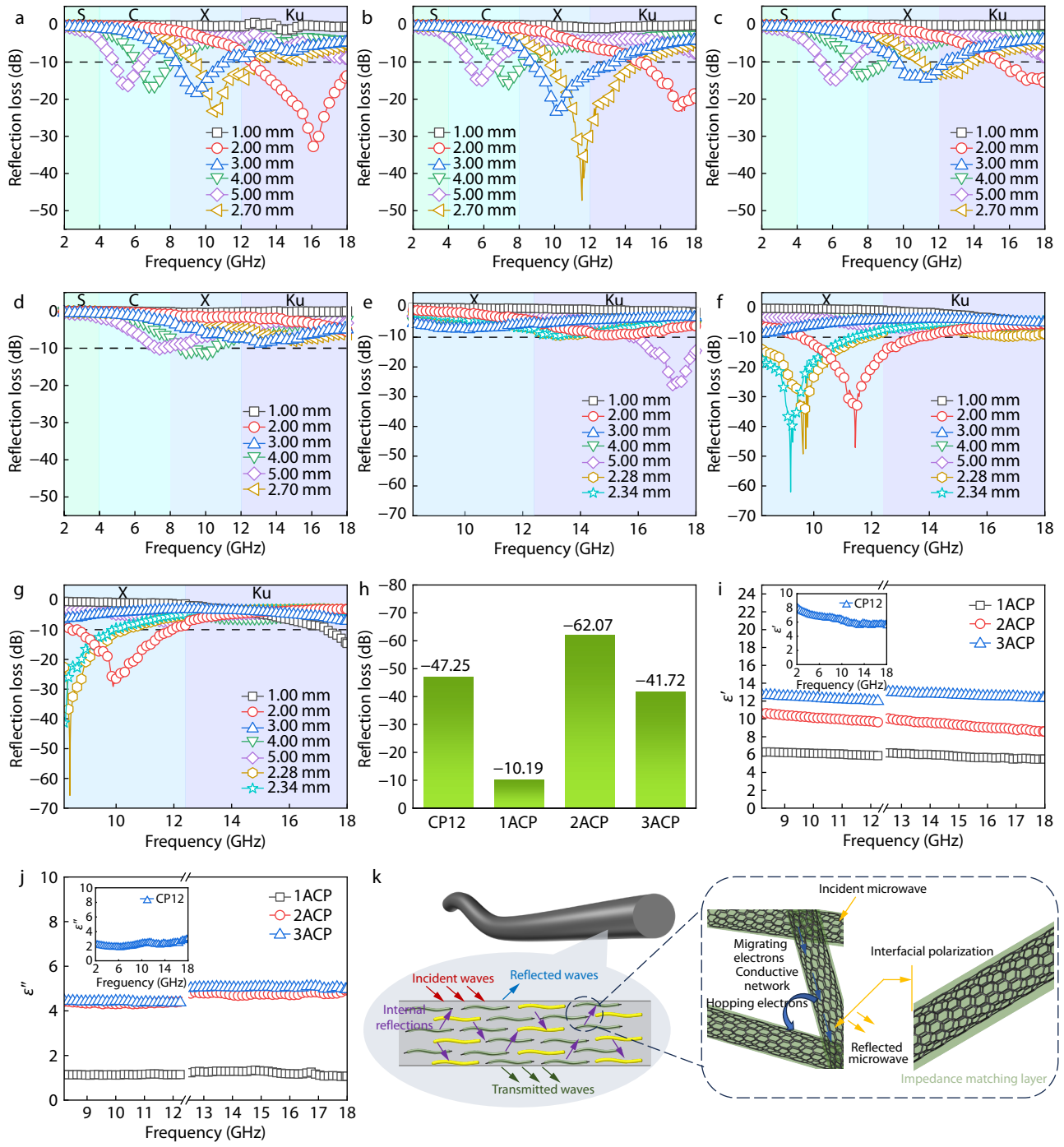

Fig. 6 2D reflection loss maps of (a) CP11, (b) CP12, (c) CP14, (d) CP18, (e) 1ACP, (f) 2ACP, and (g) 3ACP; (h) Reflection loss of samples; Complex permittivity: (i) real part, (j) imaginary part of the composite fiber; (k) Absorption mechanism schematic of the composite fiber.

conductivity and strengthens the conductive loss, which is a primary dissipation mechanism. Notably, the fiber samples achieve superior reflection loss and EAB compared to their powder counterparts, even at lower filler loadings (Fig. 6h). This enhancement is primarily attributed to the high aspect ratio of the fibrous structure, which creates extended propagation pathways and enables multiple scattering within the fiber network. As observed in Figs. 6(i) and 6(j), both the real (ε') and imaginary parts (ε'') of the permittivity increase significantly with increasing MWCNT/PANI content, reflecting the progressive formation of a more continuous conductive network within the fibers. Notably, when the mass ratio of CP12 to ANF exceeds 2:1, the fiber samples display higher ε' and ε'' values than the powder samples, further indicating an enhanced dielectric response. Additionally, the increased number of heterogeneous interfaces (MWCNT/PANI and PANI/ANF) in the composite fibers induces stronger interfacial and dipolar polarization, contributing to the elevated

complex permittivity and overall electromagnetic wave dissipation capability.[38] Importantly, beyond the enhanced dielectric response, the 2ACP fiber realizes better *Z* values (2.34 mm close to 1 while retaining a sufficiently high *α* compared to 1ACP with lower *α* and 3ACP with mismatched impedance. This balanced synergy between impedance matching and attenuation capability constitutes the fundamental reason why the 2ACP fiber exhibits the best electromagnetic wave absorption performance (RL_{min}=−62.07 dB) among all the composite fibers. This synergistic optimization of impedance matching and attenuation endows the 2ACP fiber with superior electromagnetic wave-absorption performance.

Consequently, the electromagnetic wave absorption mechanism of the ACP composite fibers mainly arises from multiple scattering and conduction loss, as illustrated in Fig. 6(k). First, MWCNTs and PANI collaboratively construct a dual-conductive network structure. Under the influence of an electromagnetic field, electrons in the MWCNTs migrate across heterogeneous interfaces to the conductive PANI layer, generating abundant microcurrents and thereby enhancing conduction loss.[39] Secondly, numerous heterogeneous interfaces such as MWCNT/PANI and PANI/ANF exist within the composite fiber, inducing interfacial polarization loss and further enhancing its dielectric loss capability. Finally, the high aspect ratio of the ACP fibers significantly extends the electromagnetic wave attenuation path.

CONCLUSIONS

ANF/MWCNT/PANI composite fibers are successfully fabricated *via in situ* polymerization and wet-spinning techniques. The controlled polymerization of PANI onto the MWCNT surface establishes a synergistic dual-conductive network, which effectively suppresses the skin effect and alleviates the impedance mismatch, thereby substantially enhancing the electromagnetic wave absorption performance. Meanwhile, the resulting 2ACP composite fibers exhibit excellent mechanical properties with a tensile strength of (202.0±8.0) MPa and an elongation at break of 13.6%±0.9%, while maintaining stable electrical conductivity. The 2ACP composite fiber achieves an RL_{min} of −62.07 dB at a thickness of 2.34 mm, and an EAB of 3.24 GHz ranging from 8.20 11.43 GHz. Additionally, the composite fibers show self-extinguishing behavior upon combustion, demonstrating their flame-retardant capability. This integrated design, combining tunable impedance matching, efficient interfacial polarization, and structural reinforcement, offers a promising and scalable strategy for flexible electromagnetic protection and next-generation wearable electronics.

Conflict of Interests

The authors declare no interest conflict.

Electronic Supplementary Information

Electronic supplementary information (ESI) is available free of charge in the online version of this article at http://doi.org/10.1007/s10118-026-3727-1.

Data Availability Statement

The data supporting the findings of this study are available from the corresponding author upon reasonable request.

ACKNOWLEDGMENTS

This work was financially supported by the Fundamental Research Funds of Zhejiang Sci-Tech University (Nos. 24212087-Y and 23212202-Y).

REFERENCES

1 Cao, Y.; Zhao, Z. Z.; Zeng, X. F.; Teng, J. X.; Huang, J. T.; Min, Y. G. High-performance polyimide/polypyrrole-CNTs@PEG composites for integrated thermal management and enhanced electromagnetic wave absorption. *Adv. Compos. Hybrid Mater.* **2025**, *8*, 104.
2 Zhu, H. H.; Liang, J.; Chen, J. F.; Chang, H.; Jiao, X. G.; Jiao, Q. G.; Feng, C. H.; Li, H. S.; Zhang, Y. Y.; Zhao, Y. Rational construction of yolk-shell structured Co_3Fe_7/FeO@carbon composite and optimization of its microwave absorption. *J. Colloid Interface Sci.* **2022**, *626*, 775−786.
3 Cheng, J. B.; Zhao, H. B.; Zhang, A. N.; Wang, Y. Q.; Wang, Y. Z. Porous carbon/Fe composites from waste fabric for high-efficiency electromagnetic wave absorption. *J. Mater. Sci. Technol.* **2022**, *126*, 266−274.
4 Meng, Y. X.; Zhang, Z.; Hou, X. G.; Wang, T.; Guo, X. Q.; Liu, X. Q.; Tian, M. W.; Qu, L. J.; Zhang, X. S. Flexible and ultra-thin graphene@MXene@Fe_3O_4 composites with excellent microwave absorption performance. *Ceram. Int.* **2024**, *50*, 6624−6633.
5 Han, H.; Lou, Z. C.; Wang, Q. Y.; Xu, L.; Li, Y. J. Introducing rich heterojunction surfaces to enhance the high-frequency electromagnetic attenuation response of flexible fiber-based wearable absorbers. *Adv. Fiber Mater.* **2024**, *6*, 739−757.
6 Wei, H.; Li, W. H.; Bachagha, K. Component optimization and microstructure design of carbon nanotube-based microwave absorbing materials: a review. *Carbon* **2024**, *217*, 118651.
7 Zeng, X. J.; Cheng, X. Y.; Yu, R. H.; Stucky, G.D. Electromagnetic microwave absorption theory and recent achievements in microwave absorbers. *Carbon* **2020**, *168*, 606−623.
8 Bao, W. L.; Liu, Y. J.; Zhao, X, M. Multiple birds with one stone: A new type of PPy/Fe_3O_4/rGO multifunctional composite fabric for wave absorption, UV resistance, anti-static and thermal insulation. *Prog. Org. Coat.* **2024**, *192*, 108465.
9 Wang, J.; Hu, Q.; Huang, J. H.; Li, J.; Lu, Y. H.; Liang, T. X.; Sheng, B.; Zheng, W. G.; Song, W. J. Multifunctional textiles enabled by simultaneous interaction with infrared and microwave electromagnetic waves. *Adv. Mater. Interfaces* **2022**, *9*, 2102322.
10 Zhou, B. B.; Zhao, X. M.; Liu, Y. J. Simple preparation of multifunctional PEDOT-based composites for wearable smart textiles. *Mater. Today Nano* **2024**, *27*, 100502.
11 Liu, Y. L.; Geng, W. Z.; Wang, L. N.; Wang, H. L.; Zhang, R.; Lan, D.; Fan, B. B. Designing MXene hydrogels for flexible and high-efficiency electromagnetic wave absorption using digital light processing 3D printing. *Chem. Eng. J.* **2025**, *505*, 159489.
12 Dong, C. L.; Li, D. C.; Wang, H. Y.; Cai, B.; Xin, Y.; Peng, H. L.; Zhao, Y.; Wang, N.; Cui, Z. M.; Wang, G. S. $CoSe_2$@ polythiophene core-shell composites with enhanced interfacial polarization for high-performance broadband electromagnetic absorption. *Carbon* **2023**, *215*, 118459.
13 He, M. J.; Tang, J. L.; Wang, Y. C.; Huang, L. Q.; Wang, X. L.; Yu, J. Y. Controlled growth of polyaniline nanofibers on the surface of alkali pre-treated PI fabric as electromagnetic wave-absorbing

Graphical Abstract

High-strength and Electrically Stable Aramid Nanofibers/Multi-walled Carbon Nanotubes/Polyaniline Hybrid Fibers for Flexible Electromagnetic Absorption Performance

Xiao-Qi Ni, Xiang-Yang Xu, Yao-Feng Zhu, and Hui-Ya Wang

Zhejiang Sci-Tech University

A flexible and robust electromagnetic-absorbing fiber is successfully fabricated *via* wet spinning techniques, which integrates multi-walled carbon nanotubes (MWCNTs), polyaniline (PANI), and aramid nanofibers (ANFs). The resulting fibers presents excellent electromagnetic wave absorption performance, mechanical properties and electrical stability.

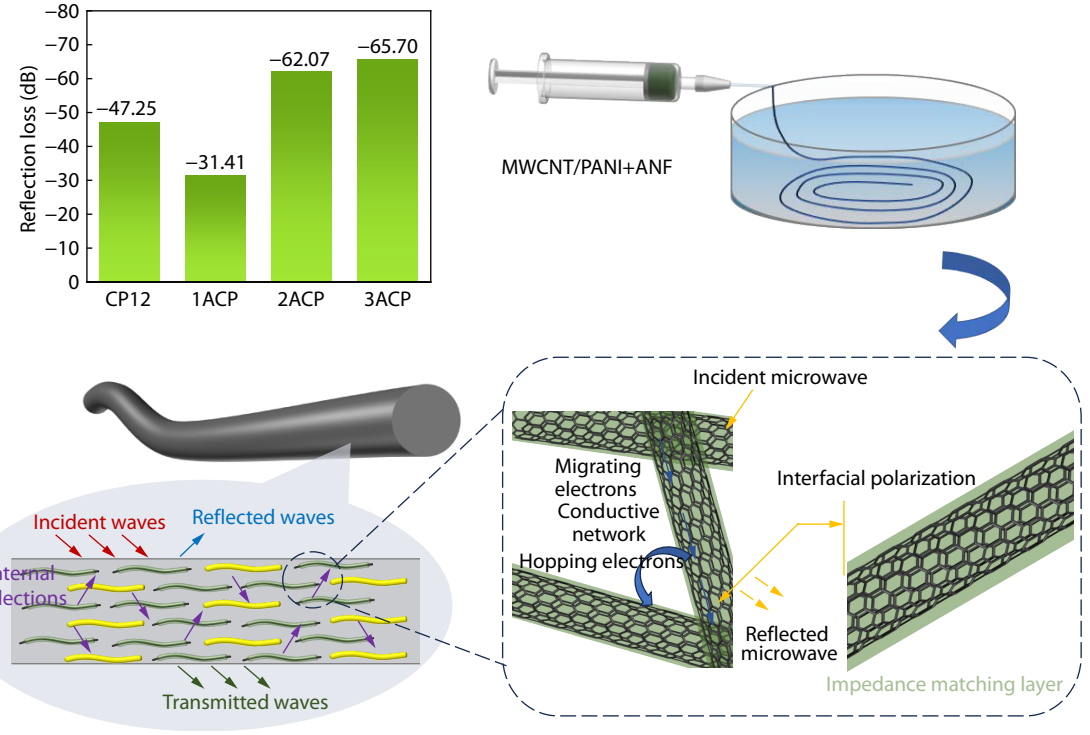

Chinese J. Polym. Sci. 2026 *https://doi.org/10.1007/s10118-026-3727-1*

fabrics. *Surf. Interfaces* **2024**, *48*, 104367.

14 Ma, J. L.; Ren, H. D.; Liu, Z. Y.; Zhou, J.; Wang, Y. Q.; Hu, B.; Liu, Y.; Kong, L. B.; Zhang, T. S. Embedded MoS_2-PANI nanocomposites with advanced microwave absorption performance. *Compos. Sci. Technol.* **2020**, *198*, 108239.

15 Sun, F. Q.; Tian, M. W.; Sun, X. T.; Xu, T. L.; Liu, X. Q.; Zhu, S. F.; Zhang, X. J.; Qu, L. J. Stretchable conductive fibers of ultrahigh tensile strain and stable conductance enabled by a worm-shaped graphene microlayer. *Nano Lett.* **2019**, *19*, 6592–6599.

16 Sun, J.; Wang, L. M.; Yang, Q.; Shen, Y.; Zhang, X. Preparation of copper-cobalt-nickel ferrite/graphene oxide/polyaniline composite and its applications in microwave absorption coating. *Prog. Org. Coat.* **2020**, *141*, 105552.

17 Wang, H.; Liu, Y.; Zhao, X. Flexible and firm multilayer $BaFe_{12}O_{19}$/GO coated composite fabric for high-performance electromagnetic shielding and wave absorption. *Prog. Org. Coat.* **2024**, *195*, 108676.

18 Kwak, B. S.; Jeong, G. W.; Choi, W. H.; Nam, Y. W. Microwave-absorbing honeycomb core structure with nickel-coated glass fabric prepared by electroless plating. *Compos. Struct.* **2021**, *256*, 113148.

19 Liu, C. C.; Li, X. L.; Li, X. Q.; Xu, T. Z.; Song, C. Y.; Ogino, K. J.; Gu, Z. J. Preparation of conductive polyester fibers using continuous two-step plating silver. *Materials* **2018**, *11*, 2033.

20 Gong, R. X.; Dong, Y. J.; Ge, D.; Miao, Z. Y.; Yu, H.Y. Wet spinning fabrication of robust and uniform intrinsically conductive cellulose nanofibril/silk conductive fibers as bifunctional strain/humidity sensor in potential smart dressing. *Adv. Fiber Mater.* **2024**, *6*, 993–1007.

21 Liu, W. W.; Xue, C.; Long, X. Y.; Ren, Y.; Chen, Z.; Zhang, W. Highly flexible and multifunctional CNTs/TPU fiber strain sensor formed in one-step *via* wet spinning. *J. Alloys Compd.* **2023**, *948*, 169641.

22 Zhao, S. Q.; Wan, A. L.; He, H. J.; Liu, Q.; Zheng, P. X.; Cong, H. L. Continuous wet-spinning of TPU composite fibers for wearable

knitted sensors. *ACS Appl. Nano Mater.* **2024**, *7*, 7052−7062.
23 Chen, X. J.; Liu, H. Y.; Hu, D. C.; Liu, H. Q.; Ma, W. S. Recent advances in carbon nanotubes-based microwave absorbing composites. *Ceram. Int.* **2021**, *47*, 23749−23761.
24 Kolanowska, A.; Janas, D.; Herman, A. P.; Jędrysiak, R. G.; Giżewski, T.; Boncel, S. From blackness to invisibility-carbon nanotubes role in the attenuation of and shielding from radio waves for stealth technology. *Carbon* **2018**, *126*, 31−52.
25 Huang, J. Z.; Li, J. Y.; Xu, X. X.; Hua, L.; Lu, Z. Q. In situ loading of polypyrrole onto aramid nanofiber and carbon nanotube aerogel fibers as physiology and motion sensors. *ACS Nano* **2022**, *16*, 8161−8171.
26 Wang, S. F.; Guo, X.; Liao, S. Q.; Chen, J. F.; Wei, Q. F. Aramid nanofiber-reinforced MXene/PEDOT:PSS hybrid fibers for high-performance fiber-shaped supercapacitors. *Electrochim. Acta.* **2023**, *466*, 143062.
27 Yang, B.; Wang, L.; Zhang, M. Y.; Luo, J. J.; Ding, X. Y. Timesaving, high-efficiency approaches to fabricate aramid nanofibers. *ACS Nano* **2019**, *13*, 7886−7897.
28 Tang, J. Y.; Li, T.; Liu, Q.; Du, J. N.; Li, J. T.; Qi, Q.; Meng, F. B. Flexible microwave absorbing fabrics woven by high-strength graphene-based hybrid fibers with broadband electromagnetic response. *J. Mater. Sci. Technol.* **2024**, *200*, 93−103.
29 Li, M. M.; Chen, X.; Li, X. T.; Dong, J.; Teng, C. Q.; Zhao, X.; Zhang, Q. H.. Ultralight aerogel textiles based on aramid nanofibers composites with excellent thermal insulation and electromagnetic shielding properties. *Compos. Commun.* **2022**, *35*, 101346.
30 Fan, B. B.; Zeng, X. J.; Fan, X. M.; Huang, X. X. Editorial for the special issue on frontiers in advanced ceramic materials for microwave absorption. *J. Adv. Ceram.* **2025**, *14*, 9221215.
31 Liu, L. X.; Chen, W.; Zhang, H. B.; Ye, L.; Wang, Z.; Zhang, Y.; Min, P.; Yu, Z. Z. Super-Tough and environmentally stable aramid. nanofiber@MXene coaxial fibers with outstanding electromagnetic interference shielding efficiency. *Nano-Micro Lett.* **2022**, *14*, 111.
32 Qiu, H.; Wang, J.; Qi, S. H.; He, Z.; Fan, X.; Dong, Y. Q. Microwave absorbing properties of multi-walled carbon nanotubes/polyaniline nanocomposites. *J. Mater. Sci.: Mater. Electron.* **2015**, *26*, 564−570.
33 Zhang, X. M.; Deng, J. H.; Yang, C. L.; Wang, Z. L.; Liu, Y. Selective reduction of nitrite to nitrogen by polyaniline-carbon nanotubes composite at neutral pH. *Environ. Res.* **2022**, *214*, 114203.
34 Wang, Z. Y.; Zhu, Y. J.; Chen, Y. Q.; Yu, H. P.; Xiong, Z. C. Flexible nanocomposite paper with superior fire retardance, mechanical properties and electrical insulation by engineering ultralong hydroxyapatite nanowires and aramid nanofibers. *Chem. Eng. J.* **2022**, *444*, 136470.
35 Fu, W. W.; Yang, W. T.; Qian, C.; Fu, Y. Q.; Zhu, Y. F. One-pot synthesis of Ag/AgCl heterojunction nanoparticles on polyaniline nanocone arrays on graphene oxide for microwave absorption. *ACS Appl. Nano Mater.* **2023**, *6*, 3728−3737.
36 Zhang, F.; Cui, W.; Wang, B. B.; Xu, B. H.; Liu, X. H.; Liu, X. H.; Jia, Z. R.; Wu, G. L. Morphology-control synthesis of polyaniline decorative porous carbon with remarkable electromagnetic wave absorption capabilities. *Compos. Part B Eng.* **2021**, *204*, 108491.
37 Li, Y.; Zhang, M. Y.; Chen, J. N.; Liu, X. H.; Huang, M.; Liu, C. T.; Shao, J.; Wang, H. L.; Fan, B. B.; Qing, Y. C. Ceramic-based electromagnetic interference shielding materials: mechanisms, optimization strategies, and pathways to next-generation applications. *J. Adv. Ceram.* **2025**, *14*, 9221194.
38 Li, M. R.; Li, W.; Wang, Y. X.; Sun, F.; Wang, Q.; Tan, D. L.; Zhang, R.; Wang, H. L.; Shao, G.; Liu, Y. L.; Fan, B. B. Entropy-driven microwave absorption enhancement in hexagonal $(Ba_{1/3}Sr_{1/3}Ca_{1/3})$ FeO_3 perovskite. *J. Adv. Ceram.* **2025**, *14*, 9221059.
39 Wang, Y. Y.; Sun, W. J.; Lin, H.; Gao, P. P.; Gao, J. F.; Dai, K.; Yan, D. X.; Li, Z. M. Steric stabilizer-based promotion of uniform polyaniline shell for enhanced electromagnetic wave absorption of carbon nanotube/polyaniline hybrids. *Compos. Part B Eng.* **2020**, *199*, 108309.